JACS
JOURNAL OF THE AMERICAN CHEMICAL SOCIETY
Article
pubs.acs.org/JACS

Sulfamic Acid-Catalyzed Lead Perovskite Formation for Solar Cell Fabrication on Glass or Plastic Substrates

Yunlong Guo,* Wataru Sato, Kazutaka Shoyama, and Eiichi Nakamura*

Department of Chemistry, The University of Tokyo, 7-3-1 Hongo, Bunkyo-ku, Tokyo 113-0033, Japan

Supporting Information

ABSTRACT: Lead perovskite materials such as methylammonium triiodoplumbate(II) ($CH_3NH_3PbI_3$, PV) are promising materials for printable solar cell (SC) applications. The preparation of PV involves a series of energetically costly cleavages of the μ-iodo bridges via conversion of a mixture of PbI_2 (PI) and methylammonium iodide (CH_3NH_3I, MAI) in *N*,*N*-dimethylformamide (DMF) into a precursor solution containing a polymeric strip of a plumbate(II) dimer $[(MA^+)_2(PbI_3^-)_2{\cdot}(DMF)_2]_m$, which then produces a perovskite film with loss of DMF upon spin-coating and heating of the substrate. We report here that the PI-to-PV conversion and the PV crystal growth to micrometer size can be accelerated by a small amount of zwitterionic sulfamic acid (NH_3SO_3, SA) and that sulfamic acid facilitates electron transfer to a neighboring electron-accepting layer in an SC device. As a result, an SC device on indium tin oxide (ITO)/glass made of a 320 nm thick PV film using 0.7 wt % SA showed a higher short-circuit current, open-circuit voltage, and fill factor and hence a 22.5% higher power conversion efficiency of 16.02% compared with the device made without SA. The power conversion efficiency value was reproducible (±0.3% for 25 devices), and the device showed very small hysteresis. The device without any encapsulation showed a respectable longevity on a shelf under nitrogen under ambient light. A flexible device similarly fabricated on ITO/poly(ethylene naphthalate) showed an efficiency of 12.4%.

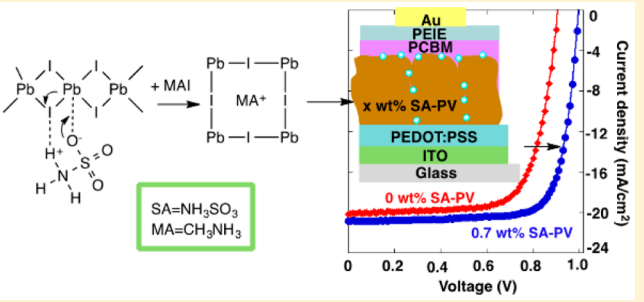

INTRODUCTION

Organic−inorganic hybrid lead perovskite (PV) attracted chemists' interest from the 1970s[1] through the 1990s,[2] and their interest has shifted to its solar cell (SC) applications[3−10] after 2009.[11] Numerous tuning methods for optimization of PV materials for SC applications notwithstanding, little was known about the chemical mechanism behind such tuning;[12] however, this mechanism was elucidated recently (Figure 1a).[13] For instance, starting from PbI_2, CH_3NH_3I (MAI), and *N*,*N*-dimethylformamide (DMF), the formation of an archetypal PV material, methylammonium triiodoplumbate(II) ($CH_3NH_3PbI_3$), involves a series of energetically costly cleavages of the μ-iodo bridges (e.g., red wavy lines in Figure 1a) such as conversion of the two-dimensional (2-D) sheet in a PbI_2 crystal into a polymeric strip of a dimer, $[(PbI_2)_2{\cdot}(DMF)_2]_n$ (**INT1**) and further degradation into shorter polymers in DMF (i.e., *n* becomes smaller). Further conversion of this dimer into a polymeric strip of a plumbate(II) dimer $[(MA^+)_2(PbI_3^-)_2{\cdot}(DMF)_2]_m$ (**INT2**)[14] is quick because it merely involves a ligand exchange. Spin coating and heating on a substrate removes DMF from **INT2** to form a cubic PV crystal. Ostwald ripening via reversible dissociation/association of DMF for **INT2** and PV causes fusion and growth of the initially formed fiber crystals of PV into large crystals.[13] Noticing that both of these slow steps involve Pb−I−Pb bond cleavage, we conjectured that a six-centered catalysis by a zwitterionic acid (Figure 1b) could accelerate these steps and hence the overall reaction. We report here that sulfamic acid (NH_3SO_3, SA) accelerates the conversion of PI into PV precursors in DMF, conversion of the latter to PV crystals, and growth of large PV crystals on the substrate. We also report that SA facilitates electron transfer from a photoexcited PV film to a neighboring electron-accepting layer (ETL) in an SC device. The latter effect is probably related to the ability of SA to raise the energy levels of the valence band (VB) and conduction band (CB) of the PV film without affecting the band gap (Figure 2b). SA is an acid (pK_a = 0.99) that is widely used in industry and in household chemicals.[15] A catalytic amount of SA (0.7 wt %) not only shortens the time required for preparation of a precursor solution from several hours to 30 min at 65 °C but also accelerates PV formation after spin-coating on a poly(3,4-ethylenedioxythiophene):polystyrenesulfonate (PEDOT:PSS) surface. Such rate acceleration effects have not been reported for previously reported acidic additives for PV film tuning (e.g., aqueous HI or hypophosphonic acid).[16] SA also facilitates the growth of large crystals (e.g., μm size in a 320 nm thick film).

A device on indium tin oxide (ITO)/glass made of a 320 nm thick PV film using 0.7 wt % SA (Figure 2c) showed a higher short-circuit current (J_{sc}), open-circuit voltage (V_{oc}), and fill factor (FF) and hence a 22.5% higher power conversion

Received: February 26, 2016
Published: April 7, 2016

DOI: 10.1021/jacs.6b02130
J. Am. Chem. Soc. 2016, 138, 5410−5416

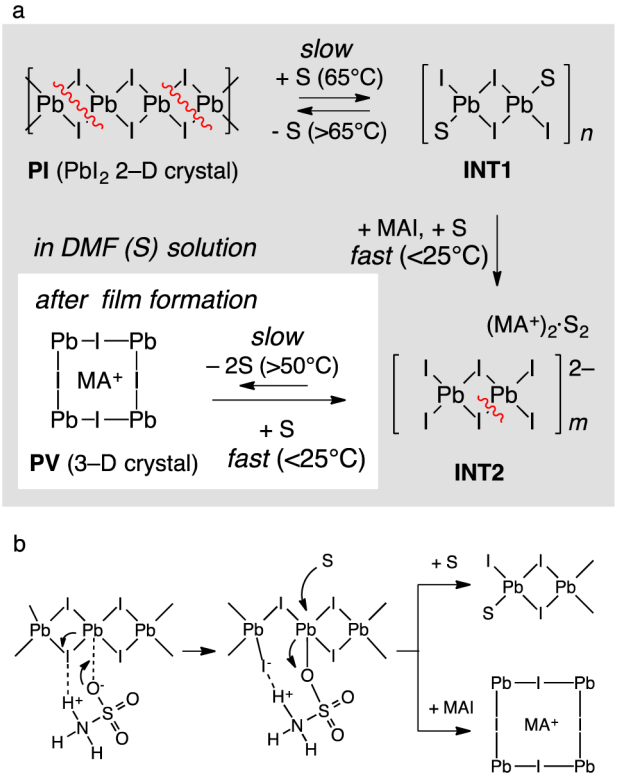

Figure 1. Mechanism of conversion of PI to PV. (a) Reported pathway for conversion of PI into intermediates in DMF and into PV after spin-coating.[13] (b) Proposed six-center catalysis by a zwitterionic acid.

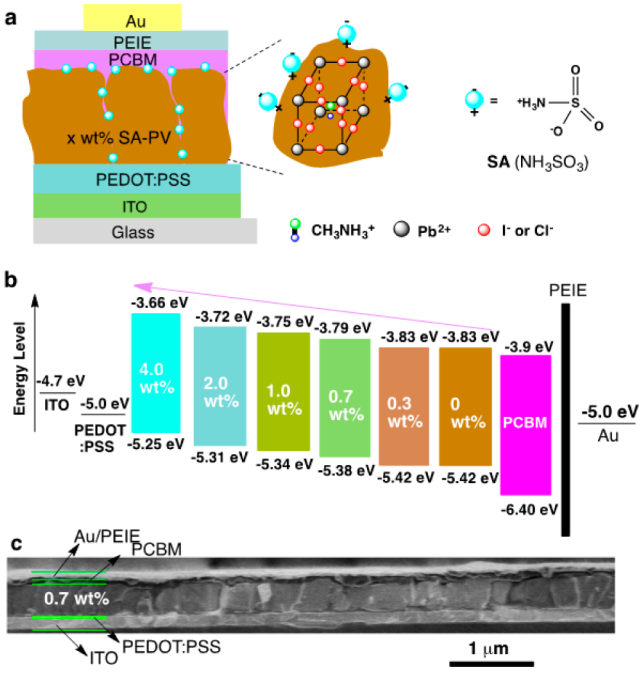

Figure 2. SA doping of PV SCs. (a) Schematic diagram of PV SC devices and surface modification by SA. (b) Energy levels of 320 nm thick PVs doped with x wt % SA. (c) Cross-sectional SEM image of an SC device made of 0.7 wt % doped SC–PV.

efficiency (PCE) of 16.02% compared with the device made without SA. The PCE value was reproducible (±0.3%), and the device showed very small hysteresis. A flexible device similarly fabricated on ITO/poly(ethylene naphthalate) (PEN) showed a PCE of 12.4%. The performance of the 16.0% PCE device without encapsulation decreased only to 13.8% after 81 days in a nitrogen glovebox under ambient light.

RESULTS AND DISCUSSION

1. SA-Accelerated Formation of PV and Device Fabrication. The perovskite material was prepared in a conventional manner and analyzed by UV–vis absorption and emission spectroscopy, photoelectron yield spectroscopy (PYS), time-of-flight secondary ion mass spectrometry (TOF–SIMS), and scanning electron microscopy (SEM) accompanied by energy dispersive X-ray spectroscopy (EDX). PYS is a recently developed method for determining the VB energy level of a semiconducting material.[17] By combining this with band-gap data estimated from the absorption onset, we determined the CB level.

A 4:1:1 molar mixture of dry crystalline MAI, PbI_2, and $PbCl_2$ was placed in DMF along with x wt % SA relative to DMF (x = 0, 0.3, 0.7, 1, 2, 4).[18] It should be noted that wording such as "0.7 wt % SA–PV" or "0.7 wt % SA doping" indicates the initial doping ratio rather than the doping ratio in the final PV film. The concentration of the precursors excluding SA was kept constant at 25 or 40 wt %. The 25 wt % formulation was used to prepare PV films with thicknesses of 100 nm (spin-coating at 5000 rpm) and 140 nm (3000 rpm), while the 40 wt % formulation was used to prepare a 320 nm thick film (3000 rpm).

It has been commonly observed that heating above 65 °C for several hours is necessary to obtain a precursor solution suitable for device fabrication.[19] Using a shorter reaction time significantly reduces the device performance, presumably because intermediates of optimum molecular weight (cf. **INT2**) are not yet produced in the precursor solution (attempts to perform light scattering analysis of the size of solute were unsuccessful because of high concentration). In the presence of 0.7 wt % SA, however, we obtained a high-performance precursor solution after heating at 65 °C for 30 min. SA doping caused a slight coloration of the precursor solution, as supported by the appearance of a weak visible absorption below 680 nm (Figure 3a,b). Interestingly, we noted that the precursor solution deteriorates after standing for half a day, as judged by a decrease in PCE, and we speculate that SA promotes further degradation of the polymeric intermediate $[(MA^+)_2(PbI_3^-)_2\cdot(DMF)_2]_n$ (**INT2**) into smaller fragments (i.e., small n) that cannot readily form PV crystals.

SA was found also to accelerate PV formation from the precursor solution on a PEDOT:PSS surface. Thus, a considerable amount of PV forms after only 5 min of spin-coating at 25 °C, as evidenced by the UV–vis spectrum and X-ray diffraction (XRD) pattern of the film (Figure 3c,d). The XRD patterns shown in Figure 3d indicate that PV crystals were formed from both $CH_3NH_3PbI_3$ (PV-I) and $CH_3NH_3PbCl_3$ (PV-Cl) in the absence of SA (blue line), whereas PV-I crystals dominated in the presence of 0.7 wt % SA–PV (red line).[9] It should be noted that after complete PV formation by heating at 100 °C, 98.3% of the PV crystals in the film consisted of PV-I (see below).

On the x wt % SA–PV films thus prepared, a 70 nm thick phenyl-C_{61}-butyric acid methyl ester (PCBM) layer was spin-coated (using chlorobenzene as the solvent), followed by coating with polyethylenimine (PEIE), an interface modification layer (in methanol).[20] Gold electrode deposition completed the SC devices. These SCs with x wt % SA–PV

DOI: 10.1021/jacs.6b02130
J. Am. Chem. Soc. 2016, 138, 5410–5416

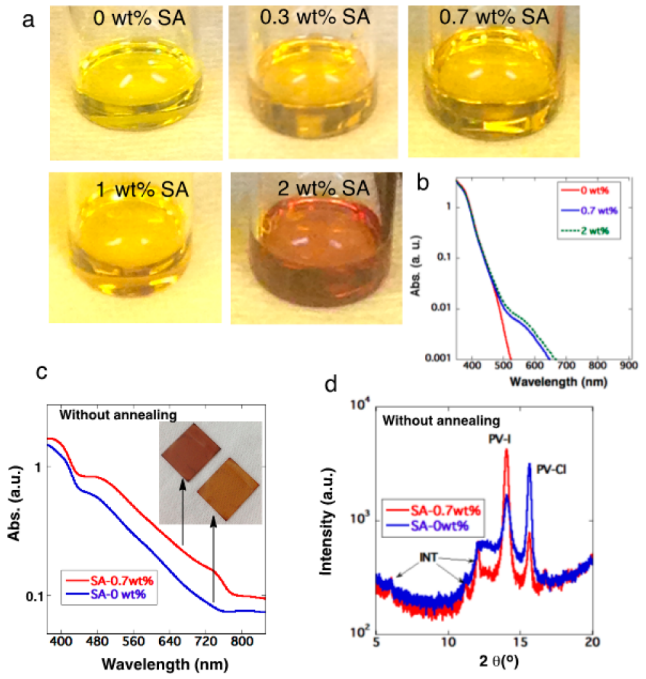

Figure 3. Effects of SA on a precursor solution and on PV formation. (a) Coloration of a solution of a mixture of SA and 40 wt % 4:1:1 MAI/PbI_2/$PbCl_2$ precursor in DMF. (b) Visible spectra with absorbance shown on a logarithmic scale. (c) Visible spectra of SA-doped PV films (140 nm) measured 5 min after spin-coating of a PEDOT:PSS surface. (d) XRD patterns of the same samples as in (c).

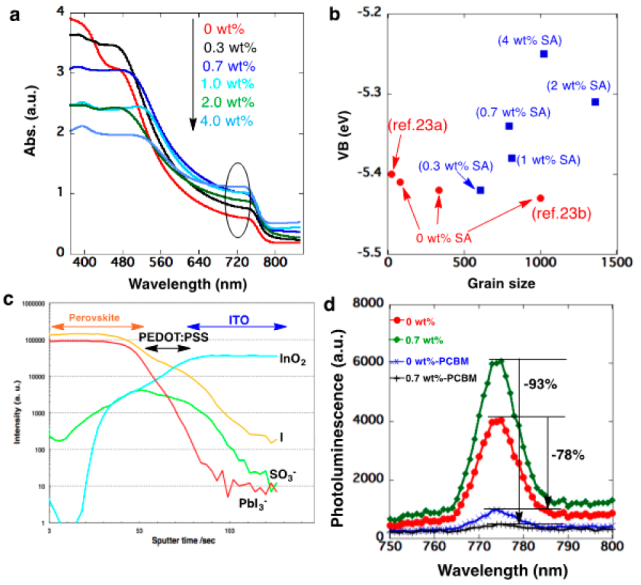

Figure 4. Characterization of PV films. (a) UV−vis spectra of different perovskite layers with a thickness of 320 nm on the ITO/PEDOT:PSS surface. (b) Relationship between grain size and VB based on different PV films. (c) TOF−SIMS data for 140 nm SA-doped PV. (d) Dependence of the PL intensity on the SA doping ratio for a PV film on glass.

are denoted as glass/ITO/PEDOT:PSS/x wt % SA−PV/PCBM/PEIE/Au, and their configuration is illustrated by the SEM-dissected image for a best-performance device with x = 0.7 wt %. The thickness of each layer is shown in Figure 2c.

2. Characterization of Perovskite Films. We first describe the physicochemical properties of the PV layers formed in the presence of x wt % SA on PEDOT:PSS. As previously noted by others and us and confirmed here by EDX (Figure S1),[21] the PV films consisted of almost pure $CH_3NH_3PbI_3$, containing only ca. 1.7% chloride anion (atom ratio = Cl/[Cl + I]) when we started from a 1:1 mixture of PbI_2 and $PbCl_2$. Selective crystallization probably sequestered MACl.

Notably, the VB level of the PV film rose from −5.42 to −5.25 eV as the SA content increased from 0 to 4 wt % (Figure 2b). For instance, 0.7 wt % SA doping raised the VB level of a 320 nm thick PV film by 0.04 eV as measured by PYS. Because PYS measures photoelectrons emitted from the surface of PV, the data suggest that the SA is located on the surface of PV crystal grains (cf. Figure 2a). Such an effect of a polar monolayer has been known since the time of Helmholtz.[17,22]

The band gap estimated from the absorption onset (779 nm =1.59 eV) was insensitive to the amount of SA (Figure 4a), and hence, the CB level also progressively rose from −3.83 to −3.66 eV with increasing x (Figures 2b and S2). The stronger absorption seen at the long-wavelength terminus (750 nm) is probably due to increased grain size (see below). As shown in Figure 4b (red dots), however, the grain size did not affect the VB level, which largely depends on the amount of doped SA.[23]

To obtain evidence of the presence of SA on the PV crystal grains, we analyzed a 0.7 wt % SA−PV film by TOF−SIMS. As shown in Figure 4c, a small amount of SA is located near the PV surface, while much of the SA is located on the grain surface in the interior of the film (it should be noted that the insensitivity of the crystal lattice to the SA content precludes incorporation of SA into the PV crystals, as discussed later).

The photoluminescence (PL) at 774 nm (Figure 4d) is informative. First, SA doping enhanced the PL, suggesting a reduction in the number of trapping sites in the SA-doped PV film.[24a,b] We ascribe this effect to the SA-assisted growth of large and well-ordered PV crystals, as evidenced below by SEM and XRD analyses. Second, SA facilitates electron transfer from a photoexcited PV film to a neighboring PCBM ETL, and hence, we expect that SA also facilitates charge collection in the SC device. Thus, spin-coating of a PCBM film on a PV film reduced the PL by 78% (Figure 4d; red line to blue line) through electron transfer from the photoexcited PV. The same experiment for a 0.7 wt % SA-doped PV film resulted in as much as 93% reduction in the PL. We can consider that increased CB energy level and/or larger crystal grains (see below) caused by SA doping resulted in such effective electron transfer from PV to the PCBM layer. Therefore, we expect an increase in SC performance upon SA doping of a PV film.

3. Morphology of SA−PV. SEM analysis of the SA−PV films prepared from a 40 wt % precursor solution in DMF (Figure 5) indicated that doping with progressively larger amounts of SA (0.3−1 wt %) results in the formation of larger grains and that further doping beyond 2 wt % results in void formation because large cubic crystals form. The small and irregularly shaped crystal grains of the 0 wt % PV film disappear in the 0.7 wt % doped film, and large grain crystals of rather uniform size are formed. The square shape of these domains conforms to a cubic crystal shape, as predicted by the Bravais−Friedel−Donnay−Harker method using the single-crystal analysis data and to be experimentally examined in due course.[24c] The void area becomes prominent above 1 wt %, apparently because of the randomness of the crystal orientation.

SA assists PV crystal growth in both thin and thick films. As shown in Figure 6a−c, PV crystals without SA doping in a 140 nm film are small (50 to 150 nm) and irregular, and the

DOI: 10.1021/jacs.6b02130
J. Am. Chem. Soc. 2016, 138, 5410−5416

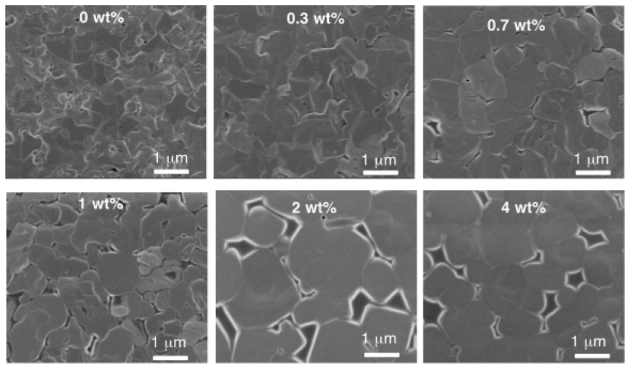

Figure 5. SEM images of x wt % SA–PV films with a thickness of 320 nm prepared from a 40 wt % precursor solution.

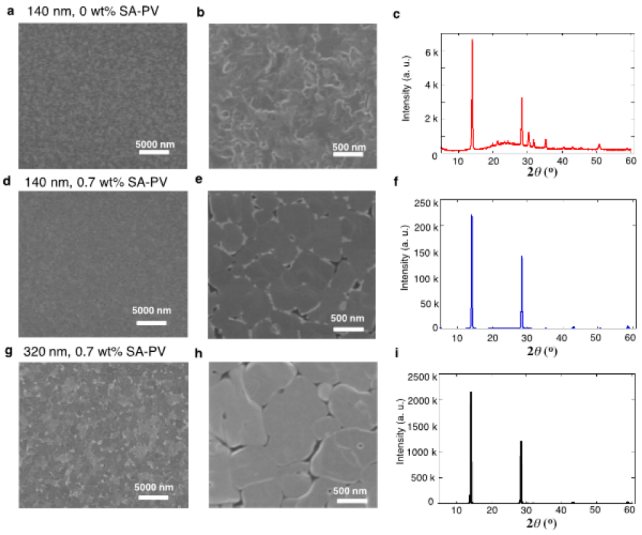

Figure 6. SEM images and XRD analysis of different perovskite materials. (a) Morphology of 140 nm thick perovskite with 0 wt % SA dopant, (b) enlarged image, and (c) its related XRD pattern. (d) Morphology of 140 nm thick perovskite with 0.7 wt % SA dopant, (e) enlarged image, and (f) its related XRD pattern. (g) Morphology of 320 nm thick perovskite with 0.7 wt % SA dopant, (h) enlarged image, and (i) its related XRD graph.

crystallinity is low, as evidenced by the weak XRD peaks found in Figure 6c. In the presence of 0.7 wt % SA (Figure 6d–f), the crystals in a 140 nm thick film become more regular and square, reminiscent of fully grown PV single crystals, and larger in size (500 ± 150 nm). Accordingly, the XRD peaks become 40 times stronger in intensity (Figure 6f, such as the first peak). When we coated a thicker film of 0.7 wt % SA–PV (320 nm thick), the crystals reached micrometer size (Figure 6g,h) and the XRD peaks were even higher (Figure 6i).

Notably, the presence of SA did not create new XRD peaks. In light of the XRD, optical band gap, PL quenching, and TOF–SIMS data, we suggest that SA is not incorporated into the PV crystal lattice but is distributed on the surface of the PV crystals and exerts dipole effects to change the VB and CB levels.

4. SCs Based on SA–PV. Finally, we describe the performance of PV SC devices with the structure glass/ITO/PEDOT:PSS/x wt % SA–PV/PCBM/PEIE/Au (Figure 2c). As shown in Figure 7 and Table 1, the best device with a 0 wt % SA–PV layer showed a PCE of 13.08%, which is similar to that reported previously.[21] When PV was doped with 0.7 wt % SA,

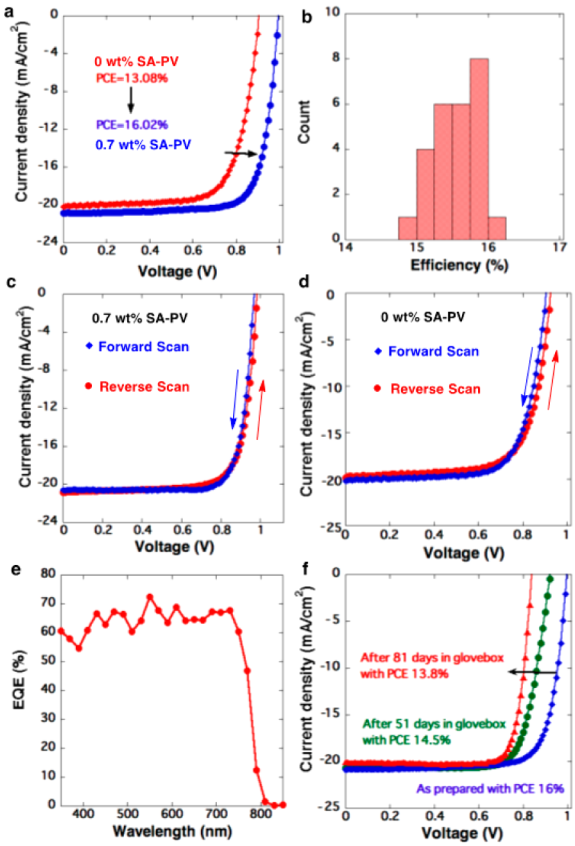

Figure 7. Performance data for SA-doped PV SC devices. (a) J–V curves with SA (blue) and without SA (red) for a 320 nm PV film. (b) PCE histogram of 25 devices with 0.7 wt % SA–PV. (c) Hysteresis of a 0.7 wt % SA–PV device. (d) Hysteresis of a device without SA doping. (e) EQE profile of the best 0.7 wt % SA–PV device. (f) J–V curves of a 0.7 wt % SA–PV device before aging and after aging under nitrogen for 51 and 81 days.

Table 1. Effects of the Dopant Weight Ratio on the Performance of SCs (All of the SCs Had 70 nm Au as the Top Electrode)

				PCE (%)	
x wt % SA–PV	J_{sc} (mA/cm^2)	V_{oc} (V)	FF (%)	best	average
0	20.21	0.906	71.3	13.08	12.4 ± 0.6
0.3	20.27	0.954	77.6	15.00	14.1 ± 0.7
0.7	20.88	0.994	77.2	16.02	15.7 ± 0.3
1.0	20.07	0.891	80.5	14.41	13.9 ± 0.4
2.0	19.69	0.879	69.8	12.09	11.1 ± 1.0
4.0	18.80	0.805	59.1	8.94	7.6 ± 1.3

the PCE increased to a best value of 16.02% (15.7% average for 25 devices; Table 1)—the same level of performance reported recently for planar-junction PV SCs using PEDOT:PSS as the hole-transporting layer and PCBM as the electron-transporting layer.[25] Thus, SA doping resulted in a 22.5% enhancement of the PCE and simultaneous improvement of all of the device parameters, e.g., J_{sc} increased from 20.21 to 20.88 mA/cm^2, V_{oc} from 0.906 to 0.994 V, and FF from 71.3% to 77.2% (Figure 7a). For 25 devices made from five batches of PV precursor solution, the PCE data reproducibly fell between 15% and 16% (Figure 7b). Hysteresis upon forward and reverse scanning of the devices was very small, which together with the above PL data suggests that the PV active layer and interfaces have a

DOI: 10.1021/jacs.6b02130
J. Am. Chem. Soc. 2016, 138, 5410–5416

negligible number of defects (Figure 7c,d). The external quantum efficiency (EQE) profile shown in Figure 7e indicates that the device absorbs the solar spectrum efficiently over a wide range. One of the devices with a Au electrode without further encapsulation showed a PCE of 16%, which became 14.5% after 51 days and 13.8% (86% of the original PCE) after 81 days in a nitrogen glovebox under ambient light (Figure 7f). The decrease in J_{sc} from 20.88 to 20.05 mA/cm^2 suggests degradation of the PV active layer, and the decrease in V_{oc} from 0.99 to 0.84 V may be ascribed to degradation of certain interfaces. The performance of the solar cell based on 0 wt % SA–PV decreased to 65% of original PCE after 81 days (see Figure S3).

SA doping is beneficial for devices using thin or thick PV films. A semitransparent thin-film PV device has promise for window applications.[23] Devices using 100–320 nm thick 0.7 wt % SA–PV showed 27–31% improvement in PCE over those using 0 wt % SA–PV because SA doping improves all three of the key parameters (J_{sc}, V_{oc}, and FF) at all thicknesses, as summarized in Figure 8 and Table S1.

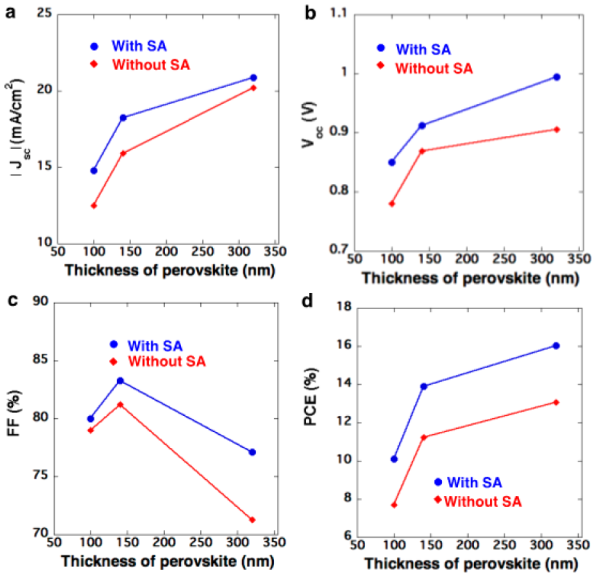

Figure 8. Effects of PV layer thickness on the performance of perovskite SCs without or with 0.7 wt % SA: (a) J_{sc}; (b) V_{oc}; (c) FF; (d) PCE.

The correlations between SA doping and device performance are summarized in Figure 9, where we find that a few factors contribute against each other so that 0.7 wt % SA doping provides the best PCE value. As shown in Figure 9a, SA doping from 0 to 4 wt % causes a steady increase in the VB and CB energy levels, which we ascribe to the modification of the interface between the PV layer and the PCBM layer by the dipole effect of the SA thin film (cf. Figure 1a). SA also has a significant impact on the crystal grain size due to SA-mediated Ostwald ripening as well as void area (Figures 4 and S4). As shown in Figure 9b, the coverage is high below 1 wt % SA doping, where the grain size is smaller than ca. 700 nm, and decreases above 1 wt % SA, where the grain size is as large as 1 μm. Comparison of Figure 9b with Figure 9c shows that the coverage and grain size are closely related to the shunt resistance (R_{sh}) and series resistance (R_s) and hence affect the FF value shown in Figure 9d. J_{sc} and V_{oc} are relatively less affected by the SA content.

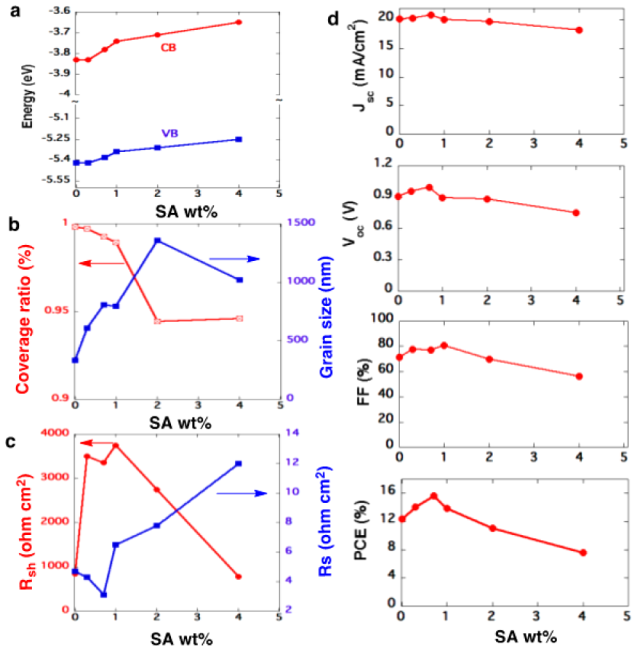

Figure 9. Correlations between the SA doping ratio and various device parameters: (a) CB and VB; (b) surface coverage by the perovskite layer and PV grain size; (c) R_{sh} and R_s; (d) J_{sc}, V_{oc}, FF, and PCE of SCs (average values).

Finally, we illustrate the feasibility of a flexible SC fabricated on PEN by a low-temperature solution process—an advantage of PEDOT:PSS as a hole-transport layer over TiO_2, which requires high-temperature annealing incompatible with an inexpensive plastic substrate. This device endures 90° bending for up to 200 cycles at room temperature (Figure 10a). The J–V curve shown in Figure 10b for the highest-performing device yielded V_{oc} = 0.96 V, J_{sc} = 19.72 mA/cm^2, FF = 65.3%, and PCE = 12.36%, which is a value comparable with data reported recently.[26]

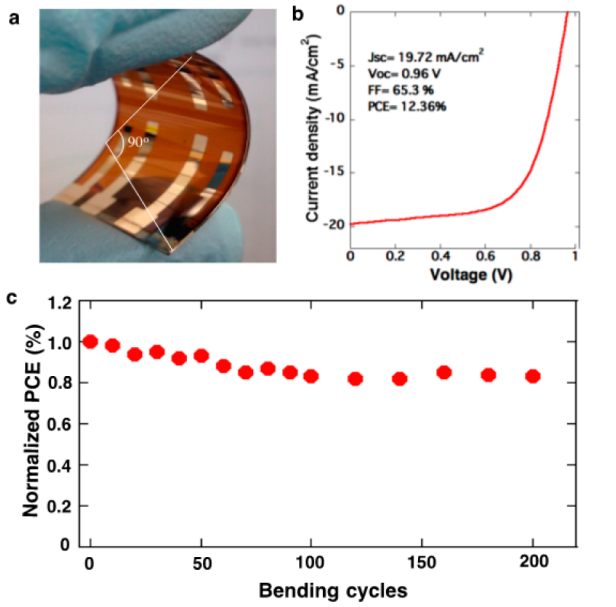

Figure 10. Characterization of an SC device using 0.7 wt % SA–PV on PEN. (a) Photograph of the flexible device. (b) J–V curve of the device. (c) Bending test of the device with a bending angle of 90°.

DOI: 10.1021/jacs.6b02130
J. Am. Chem. Soc. 2016, 138, 5410–5416

CONCLUSION

We found that the presence of a small amount of acidic SA exerts beneficial effects on the fabrication of PV for SC fabrication on glass and flexible plastic films. First, SA catalyzes Pb−I−Pb bond cleavage to shorten the time required for the preparation of the precursor solution and PV crystal formation. The large PV crystals thus formed contribute to increasing the SC performance. Second, SA doping modifies the surface property of PV crystals to facilitate electron transfer from the photoexcited PV film to an electron-accepting PCBM layer and hence increases the SC performance. SA doping at the 0.7 wt % level thus reproducibly provided high-performance SC devices, the best of which had a PCE of 16.02%, which is 22% higher than that of the device without SA doping. This device composed of micrometer-sized crystals also showed respectable stability upon standing. We expect that further studies on the mechanism of SA-catalyzed PV formation and the electronic effects of SA doping will be beneficial for the design of high-performance PV SC devices.

EXPERIMENTAL SECTION

Materials. MAI was prepared following previous reports.[27] In a glovebox (N_2 atmosphere), MAI, PbI_2 (TCI, 99.999%), $PbCl_2$ (Sigma-Aldrich, 99.999%), and NH_3SO_3 (Wako, ∼98%) were dissolved in DMF (Tokyo Chemical Industry Co., 99.5%).

Preparation of *x* wt % SA-Doped PV Precursor Solution. For 0 wt % SA−PV precursor solution, a 4:1:1 molar mixture of solid powder MAI, PbI_2, and $PbCl_2$ was placed in DMF. Then the solution was heated at 65 °C for about 12 h to form a uniform precursor solution. For SA-doped PV precursor solutions, a 4:1:1 molar mixture of solid powder MAI, PbI_2, and $PbCl_2$ along with SA (*x* wt % relative to the weight of DMF) was dissolved in DMF solvent, and the solution was heated at 65 °C for about 30 min to form the precursor solution.

UV−Vis and PL Spectra. The UV−vis spectra of the PV thin films on a PEDOT:PSS surface were recorded on a Jasco V-670 spectrophotometer. PL spectra of PV films on glass were measured using a fluorescence spectrophotometer (HITACHI F-4500).

TOF−SIMS Measurements. Mass spectrum measurement (high mass resolution mode): primary ion Bi_3^{2+}, acceleration voltage 25 kV, irradiation current 0.1 or 0.2 pA, 200 or 100 μm angle scanning, positive and negative ion measurement, 30 scan integration flood gun use. Ion image measurement (high spatial resolution mode): primary ion Bi^+, acceleration voltage 25 kV, 15 μm angle scanning, positive and negative ion measurement, 180 scan integration flood gun use. Depth profile measurement: Negative ion measurement, four or eight scan/cycle integration flood gun use, sputter ion Ar^+, acceleration voltage 2 kV, 200 μm angle scanning, 3 s/cycle irradiation.

XRD Measurements. The XRD experiments were performed on a Rigaku SmartLab X-ray diffractometer equipped with a scintillation counter. The measurements employed the Cu Kα line, focused radiation at a power of 9 kW (45 kV, 200 mA) using a 0.02° 2θ step scan from 3.0−60.0° at a scanning speed of 3° min^{-1}.

SEM and EDX Measurements. SEM observations were conducted on an FEI Magellan 400L scanning electron microscope equipped with AMETEK/EDAX Genesis APEX4 instrument at a landing voltage of 1 kV under a reduced pressure of 5×10^{-5} Pa.

Preparation of SC Devices on Glass. The devices were fabricated according to the following typical procedure. A 145 nm thick ITO layer with a sheet resistance of 8 Ω/square was deposited on a glass substrate. The patterned ITO glass was ultrasonically cleaned using a surfactant, rinsed with water, and then subjected to a 3 min UV−ozone treatment. A PEDOT:PSS solution (AI4083) was spin-coated on the ITO surface at 500 rpm for 3 s and then at 3000 rpm for 30 s in air and was annealed at 130 °C for 25 min under air and 20 min under N_2. A solution of 0−4 wt % SA−PV precursor solution was spin-coated on the PEDOT:PSS surface under a nitrogen atmosphere. The film was allowed to stand for 5 min and was then annealed at 100 °C for 25 min. An electron-transporting layer (PCBM, 30 mg/mL in chlorobenzene) was deposited by spin-coating (1000 rpm/45 s). PEIE (0.02 wt %, in methanol), an interface modification layer, was spin-coated at 6000 rpm for 30 s. The top electrode (Au, 70 nm) was deposited via a metal shadow mask.

Preparation of Flexible Devices. We used a flexible PEN substrate (Oike Kogo Co.) with patterning of ITO (200 nm, 15 Ω/square, transmittance >88%; TechnoPrint Co.) for flexible device fabrication. First, the PEN film was washed with isopropanol and treated for 10 min with UV−ozone. To avoid bending of the PEN during spin-coating, a holder for a flexible substrate (Fujikura Composites Co.) was used. PEDOT:PSS (modified by polyoxyethylene (10) tridecyl ether and DMSO with volume ratios of 0.05% and 0.5%, respectively) was spin-coated at 2000 rpm for 30 s following annealing under air (100 °C/20 min) as well as under N_2 (100 °C/20 min). A 0.7 wt % SA−PV precursor solution (40 wt %) was spin-coated on the PEDOT:PSS surface. After 5 min, the substrate was annealed at 100 °C for 25 min in N_2. A solution of 30 mg/mL PCBM in chlorobenzene was spin-coated as the ETL followed by PEIE as the interface modification layer. Finally, 70 nm Au was deposited in a vacuum chamber to form the electrode.

Evaluation of PV Devices. Current−voltage sweeps were performed using a Keithley 2400 source measurement unit controlled by a computer. The light source used to determine the PCE was an AM 1.5G solar simulator system (Sumitomo Heavy Industries Advanced Machinery) with an intensity of 100 mW/cm^2. The SCs were masked with a metal aperture to define the active area of 4 mm^2.

ASSOCIATED CONTENT

Supporting Information

The Supporting Information is available free of charge on the ACS Publications website at DOI: 10.1021/jacs.6b02130.

Details of EDX data, PYS analysis, PV grain size analysis, and effect of PV layer thickness on devices (PDF)

AUTHOR INFORMATION

Corresponding Authors

*guoyunlong@chem.s.u-tokyo.ac.jp

*nakamura@chem.s.u-tokyo.ac.jp

Notes

The authors declare no competing financial interest.

ACKNOWLEDGMENTS

We thank MEXT for financial support [KAKENHI 15H05754 and CREST, JST to E.N., the Strategic Promotion of Innovative Research, JST to Y.G.; K.S. was supported by the Japan Society for the Promotion of Science through the Program for Leading Graduate Schools (MERIT)]. We thank Mitsubishi Chemical Co. for the TOF−SIMS measurements.

REFERENCES

(1) Weber, D. *Z. Naturforsch.* **1978**, *33b*, 1443−1445.

(2) (a) Poglitsch, A.; Weber, D. *J. Chem. Phys.* **1987**, *87*, 6373−6378. (b) Xu, Q.; Eguchi, T.; Nakayama, H.; Nakamura, N.; Kishita, M. *Z. Naturforsch., A: Phys. Sci.* **1991**, *46*, 240−246. (c) Onoda-Yamamuro, N.; Yamamuro, O.; Matsuo, T.; Suga, H. *J. Phys. Chem. Solids* **1992**, *53*, 277−281. (d) Onoda-Yamamuro, N.; Matsuo, T.; Suga, H. *J. Phys. Chem. Solids* **1992**, *53*, 935−939. (e) Papavassiliou, G. C.; Koutselas, I. B. *Synth. Met.* **1995**, *71*, 1713−1714. (f) Kawamura, Y.; Mashiyama, H.; Hasebe, K. *J. Phys. Soc. Jpn.* **2002**, *71*, 1694−1697. (g) Tanaka, K.; Takahashi, T.; Ban, T.; Kondo, T.; Uchida, K.; Miura, N. *Solid State Commun.* **2003**, *127*, 619−623.

(3) Green, M.; Emery, K.; Hishikawa, Y.; Warta, W.; Dunlop, E. D. *Prog. Photovoltaics* **2015**, *23*, 805−812.

(4) Stoumpos, C. C.; Malliakas, C. D.; Kanatzidis, M. G. *Inorg. Chem.* **2013**, *52*, 9019−9038.

DOI: 10.1021/jacs.6b02130
J. Am. Chem. Soc. 2016, 138, 5410−5416

(5) Park, N.-G. *J. Phys. Chem. Lett.* **2013**, *4*, 2423−2429.
(6) Nishimura, H.; Ishida, N.; Shimazaki, A.; Wakamiya, A.; Saeki, A.; Scott, L. T.; Murata, Y. *J. Am. Chem. Soc.* **2015**, *137*, 15656−15659.
(7) (a) Liang, P.; Liao, C.; Chueh, C.; Zuo, F.; Williams, S.; Xin, X.; Lin, J.; Jen, A. *Adv. Mater.* **2014**, *26*, 3748−3754. (b) Liu, M. Z.; Johnston, M. B.; Snaith, H. J. *Nature* **2013**, *501*, 395−398.
(8) Burschka, J.; Pellet, N.; Moon, S.-J.; Humphry-Baker, R.; Gao, P.; Nazeeruddin, M. K.; Grätzel, M. *Nature* **2013**, *499*, 316−319.
(9) Zhou, H. P.; Chen, Q.; Li, G.; Luo, S.; Song, T.; Duan, H.; Hong, Z. R.; You, J. B.; Liu, Y. S.; Yang, Y. *Science* **2014**, *345*, 542−546.
(10) Jeon, N. J.; Noh, J. H.; Yang, W. S.; Kim, Y. C.; Ryu, S.; Seo, J.; Seok, S. I. *Nature* **2015**, *517*, 476.
(11) Kojima, A.; Teshima, K.; Shirai, Y.; Miyasaka, T. *J. Am. Chem. Soc.* **2009**, *131*, 6050−6051.
(12) Manser, J.; Saidaminov, M.; Christians, J.; Bakr, O.; Kamat, P. *Acc. Chem. Res.* **2016**, *49*, 330−338.
(13) Guo, Y.; Shoyama, K.; Sato, W.; Matsuo, Y.; Inoue, K.; Harano, K.; Liu, C.; Tanaka, H.; Nakamura, E. *J. Am. Chem. Soc.* **2015**, *137*, 15907−15914.
(14) Wakamiya, A.; Endo, M.; Sasamori, T.; Tokitoh, N.; Ogomi, Y.; Hayase, S.; Murata, Y. *Chem. Lett.* **2014**, *43*, 711−713.
(15) https://en.wikipedia.org/wiki/Sulfamic_acid.
(16) (a) Eperon, G.; Stranks, S.; Menelaou, C.; Johnston, M.; Herz, L.; Snaith, H. *Energy Environ. Sci.* **2014**, *7*, 982−988. (b) Zhang, W.; Pathak, S.; Sakai, N.; Stergiopoulos, T.; Nayak, P.; Noel, N.; Haghighirad, A.; Burlakov, V.; deQuilettes, D.; Sadhanala, A.; Li, W.; Wang, L.; Ginger, D.; Friend, R.; Snaith, H. *Nat. Commun.* **2015**, *6*, 10030.
(17) Lacher, S.; Matsuo, Y.; Nakamura, E. *J. Am. Chem. Soc.* **2011**, *133*, 16997−17004.
(18) Xue, Q.; Hu, Z.; Liu, J.; Lin, J.; Sun, C.; Chen, Z.; Duan, C.; Wang, J.; Liao, C.; Lau, W.; Huang, F.; Yip, H.; Cao, Y. *J. Mater. Chem. A* **2014**, *2*, 19598−19603.
(19) Li, X.; Ibrahim Dar, M.; Yi, C.; Luo, J.; Tschumi, M.; Zakeeruddin, S. M.; Nazeeruddin, M. K.; Han, H.; Grätzel, M. *Nat. Chem.* **2015**, *7*, 703−711.
(20) Zhou, Y.; Fuentes-Hernandez, C.; Shim, J.; Meyer, J.; Giordano, A. J.; Li, H.; Winget, P.; Papadopoulos, T.; Cheun, H.; Kim, J.; Fenoll, M.; Dindar, A.; Haske, W.; Najafabadi, E.; Khan, T.; Sojoudi, H.; Barlow, S.; Graham, S.; Brédas, J.; Marder, S.; Kahn, A.; Kippelen, B. *Science* **2012**, *336*, 327−332.
(21) You, J.; Hong, Z.; Yang, Y.; Chen, Q.; Cai, M.; Song, T.-B.; Chen, C.-C.; Lu, S.; Liu, Y.; Zhou, Z.; Yang, Y. *ACS Nano* **2014**, *8*, 1674−1680.
(22) Topping, J. *Proc. R. Soc. London, Ser. A* **1927**, *114*, 67−72.
(23) (a) Guo, Y.; Shoyama, K.; Sato, W.; Nakamura, E. *Adv. Energy Mater.* **2016**, *6*, 1502317. (b) Bi, C.; Wang, Q.; Shao, Y.; Yuan, Y.; Xiao, Z.; Huang, J. *Nat. Commun.* **2015**, *6*, 7747.
(24) (a) Zuo, L.; Gu, Z.; Ye, T.; Fu, W.; Wu, G.; Li, H.; Chen, H. *J. Am. Chem. Soc.* **2015**, *137*, 2674−2679. (b) Xing, G.; Mathews, N.; Sun, S.; Lim, S.; Lam, Y.; Grätzel, M.; Mhaisalkar, S.; Sum, T. *Science* **2013**, *342*, 344−347. (c) Ye, T.; Fu, W.; Wu, J.; Yu, Z.; Jin, X.; Chen, H.; Li, H. *J. Mater. Chem. A* **2016**, *4*, 1214−1217.
(25) Nie, W.; Tsai, H.; Asadpour, R.; Blancon, J.; Neukirch, A. J.; Gupta, G.; Crochet, J.; Chhowalla, M.; Tretiak, S.; Alam, M. A.; Wang, H.; Mohite, A. D. *Science* **2015**, *347*, 522−525.
(26) Kaltenbrunner, M.; Adam, G.; Głowacki, E. D.; Drack, M.; Schwödiauer, R.; Leonat, L.; Apaydin, D. H.; Groiss, H.; Scharber, M. C.; White, M. S.; Sariciftci, N. S.; Bauer, S. *Nat. Mater.* **2015**, *14*, 1032−1039.
(27) Guo, Y.; Liu, C.; Inoue, K.; Harano, K.; Tanaka, H.; Nakamura, E. *J. Mater. Chem. A* **2014**, *2*, 13827−13830.

DOI: 10.1021/jacs.6b02130
J. Am. Chem. Soc. 2016, 138, 5410−5416